Cancer tissue of origin constrains the growth and metabolism of metastases

Sharanya Sivanand[1,2], Yetis Gultekin[1,2,#], Peter S. Winter[1,3,4,5,#], Sidney Y. Vermeulen[1,2,#], Konstantine Tchourine[6], Laura V. Danai[1,2], Brian T. Do[1,5], Kayla Crowder[8], Tenzin Kunchok[8], Allison N. Lau[1,2], Alicia M. Darnell[1,2], Satoru Morita[9], Dan G. Duda[9], Andrew Aguirre[3,4,10], Brian M. Wolpin[3], Caroline A. Lewis[8], Dennis Vitkup[6,7], Alex K. Shalek[1,4,5,11,12], Matthew G. Vander Heiden[1,2,3,4*]

[1]Koch Institute for Integrative Cancer Research, Massachusetts Institute of Technology, Cambridge, MA 02139, USA

[2]Department of Biology, Massachusetts Institute of Technology, Cambridge, MA 02139, USA

[3]Department of Medical Oncology, Dana-Farber Cancer Institute, Boston, MA, 02115, USA

[4]Broad Institute of MIT and Harvard, Cambridge, MA, 02142, USA

[5]Institute for Medical Engineering and Science, Massachusetts Institute of Technology, Cambridge, MA, 02139, USA

[6]Department of Systems Biology, Columbia University Medical Center, New York, NY, 10032, USA

[7]Department of Biomedical Informatics, Columbia University Medical Center, New York, NY, 10032, USA

[8]Whitehead Institute for Biomedical Research, Cambridge, MA, 02142, USA

[9]Edwin L Steele Laboratories, Department of Radiation Oncology, Massachusetts General Hospital and Harvard Medical School, Boston, MA, 02114, USA

[10]Department of Medicine, Brigham and Women's Hospital and Harvard Medical School, Boston, MA, USA

[11]Department of Chemistry, Massachusetts Institute of Chemistry, Cambridge, MA, 02139, USA

[12]Ragon Institute of MGH, MIT, and Harvard, Cambridge, MA, 02139, USA

[#]These authors contributed equally to this work.

[*]Corresponding author. Email: mvh@mit.edu

Abstract

Metastases arise from a subset of cancer cells that disseminate from the primary tumor; however, the factors that contribute to proliferation of cancer cells in a secondary site are incompletely understood. The ability of cancer cells to thrive in a new tissue site is influenced by genetic and epigenetic changes that are important for disease initiation and progression, but these factors alone do not predict if and where cancers metastasize. Specific cancer types metastasize to consistent subsets of tissues, suggesting that factors within the primary tumor influence the tissue environments where cancers can grow. Using pancreatic cancer as a model, we find that primary and metastatic tumors are metabolically similar to each other and that the tumor initiating capacity and proliferation of both primary- and metastasis-derived cells is favored in the primary site relative to the metastatic site. Moreover, propagating lung or liver metastatic cells *in vivo* to enrich for tumor cells adapted to grow in the lung or the liver does not enhance their relative ability to form large tumors in those sites, change their preference to grow in the

primary site, nor stably alter their metabolism relative to primary tumors. To assess whether this preference for the primary site is specific to pancreatic cancer, we analyzed liver and lung cancer cells and find that these cells also best form tumors in the tissue that corresponds to their primary site. Together, these data suggest that the cancer tissue-of-origin influences the metabolism of both primary and metastatic tumors and may impact whether cancer cells can thrive in a metastatic site.

One-Sentence Summary: Tissue-of-origin is a major determinant of metastatic tumor metabolism and accessing the right metabolic environment may contribute to why cancers metastasize to specific tissues.

Metastasis contributes to the high mortality of patients with cancer. Metastases arise from a subset of cancer cell clones within the primary tumor (*1*); however, why some clones thrive in new tissue sites and what determines which tissue sites will support proliferation of metastatic cancer cells is incompletely understood. It is known that formation of metastasis is a rare event (*2*). The fact that metastases are derived from a subset of clones found in a primary tumor may suggest that only those cancer cells that are adapted to grow in the new tissue site are selected for during metastasis. Oncogenic mutations are important contributors to primary tumor initiation and disease progression (*3*), but despite extensive efforts, causal genetic determinants of metastasis have not been identified. This has led to the speculation that epigenetic alterations must be involved in allowing cancer cells to thrive in new tissue sites; however, consistent gene expression programs that predict which cancers can grow in any specific tissue have also not been

found. These data argue that genetic factors alone do not predict metastasis (*4*), and the fact that cancers arising in different tissue sites tend to metastasize to distinct subsets of tissue locations that are characteristic of that tumor type argues that some property of the primary tumor influences the specific tissues to where cancer cells can metastasize. Nevertheless, the properties of the primary tumor environment that are shared with the metastatic tumor environment to allow metastasis are not well understood.

One factor that could be shared between primary and metastatic sites and might influence whether tumors can grow in each location is nutrient availability, as metabolism is a property of cancer that is influenced by tissue environment (*5*). Genetic events, such as oncogenic *Ras* signaling, contribute to metabolic changes in cancer (*6*–*8*); however, cancer tissue-of-origin and tumor location also influence cancer metabolic phenotypes (*9*, *10*). The nutrients available to cancer cells in tumors depends on tissue location and cancer type (*11*–*13*), and it has been proposed that tumor cells exhibit metabolic plasticity to allow proliferation in a metastatic site, a model whereby metastatic tumors adapt their metabolism to deviate from the primary tumor and match that of the metastatic site (*14*, *15*). However, tumor metabolic gene expression better resembles the tissue-of-origin for a cancer than it does tumors arising in other tissues (*16*, *17*), and differences in nutrient availability across tissues might constrain the tissue of origin-shaped metabolism of cancer cells and limit where cells can thrive as metastases (*11*, *16*–*18*). This model would predict metabolic similarities between the primary and the metastatic tumors and that the metabolism of the metastatic tumor is determined by the tissue-of-origin, a possibility that has not been tested. This led us to investigate how well primary- and metastasis-derived

cancer cells can grow in different tissues, and how metastatic tumor metabolism relates to the primary tumor.

Pancreatic ductal adenocarcinoma (PDAC) has a high incidence of metastasis, and the genetically engineered *LSL-Kras$^{G12D/+}$; Trp53$^{R172H/+}$; Pdx-1-Cre* (KPC) mouse pancreatic cancer model recapitulates many features of the human disease including a propensity to metastasize (*19*, *20*). Over a period of 6-8 months, KPC mice develop tumors in the pancreas and frequently develop metastatic lesions in the liver, and occasionally in the lung (*19*), a metastatic pattern similar to that observed in patients. To study primary and metastatic PDAC cells, cancer cells were isolated from primary tumors and matched liver or lung metastases that arose in the KPC model, and that proliferated at similar rates when cultured in standard conditions in vitro (Fig. S1). To determine whether the cells derived from primary or metastatic tumors exhibit a preference to form tumors in different tissues in a mouse when competed against each other, cancer cells from matched primary tumors or liver metastases were engineered to express either mCherry or GFP, such that equal numbers of cells expressing different fluorescent proteins could be mixed and implanted into the pancreas, liver, or flank (subcutaneous) in syngeneic C57BL/6J mice (Fig. S2A). We confirmed that the labeled cell populations had approximately equivalent representation prior to implantation (Fig. S2B), and that all cells could form tumors of similar size in the pancreas when injected individually, or co-injected as a mixed population (fig. S2C). When a mixed population of cells derived from primary tumors and liver metastases were implanted in the pancreas, the resulting tumors were enriched for primary tumor-derived cells when analyzed by either flow-cytometry or

immunohistochemistry (Fig. S2D-E). When a mixed population of cells was implanted in the liver, liver metastases-derived cells were more abundant, even though primary tumor-derived cells also contributed to the resulting tumor (Fig. S2F-H). Interestingly, when a mixed population of primary- and liver metastasis-derived cells were implanted in the flank, the resulting tumor was derived primarily from one of the two cell populations (Fig. S2I). These data are consistent with tumors at either the primary or a metastatic site being derived from a subset of cancer cells, and are consistent with prior studies suggesting that cancer cells can be selected to metastasize to specific sites (*21*).

To determine whether a subset of cancer cells contributing to the bulk of the resulting tumors reflects selection for cells that are best adapted to grow in a given tissue, or whether stochastic processes related to metastasis being a rare event also contribute (*2*), we labeled the same cancer cells with either mCherry or GFP, mixed them in equal proportions (Fig. 1A), and implanted the mixed population into the pancreas, liver, or flank. Even though the different labeled cancer cells were derived from the same cell population, in most instances, either an mCherry or GFP labeled cell was found to be the dominant clone in tumors that formed regardless of site (Fig. 1B-D). These data are consistent with observations of clonal dominance in pancreatic cancer in both primary and metastatic sites (*22*), but also raise the possibility that the presence of primary tumor subclones in metastases reflects, at least in part, that relatively few cells contribute to a bulk tumor.

Several studies have noted that the availability of specific nutrients can determine whether cancer cells can thrive in a metastatic site (*23*); however, those studies have focused on how metabolism of a specific tissue metastasis might differ from a primary tumor, and a comprehensive analysis of both the metabolic similarities and differences for primary and metastatic tumors is lacking. To begin to assess whether accessing a metastatic tissue environment with sufficient similarity to the primary site is important to support the metabolism of metastatic cancer cells, we implanted primary- or liver metastasis-derived PDAC cells into the pancreas or liver to form tumors in mice. Assessment of transplanted tumors was necessary to study the metabolism of metastases, because it was not possible to isolate large enough metastatic tumors from the KPC model for functional analysis of metabolism. Assessment of implanted tumors also allows comparison of tumors within a predictable time window that enables analysis of isotopically-labeled glucose fate in tumor tissue in conscious, unrestrained tumor bearing mice (*24*). Mice were analyzed after a 6 hour ^{13}C-glucose infusion, a time where metabolite labeling approaches steady state allowing comparison of glucose fate between tissues (*24*). Similar ^{13}C-glucose enrichment was observed in plasma of labeled-glucose infused mice bearing either pancreatic tumors or liver metastatic tumors (Fig. S3A), and minimal differences in glucose fate were observed when comparing how metabolites were labeled in tumors growing in the pancreas and liver (Fig. 1E-L).

To extend these findings to a second mouse model of pancreatic cancer, we utilized cancer cells isolated from the *LSL-Kras$^{G12D/+}$; Trp53$^{-/-}$; Pdx-1-Cre* (KP$^{-/-}$C) mouse model of PDAC (*25*, *26*), and implanted those cells into the pancreas, liver, and flank to again

assess the fate of U-^{13}C glucose in tumors arising in each location, as well as in the normal pancreas and liver. While a different labeling pattern was observed when comparing metabolites from tumors to metabolites from the normal pancreas and liver, minimal differences in labeling were present in pancreatic tumors growing in different tissue sites (Fig. S3B-I). These data argue that in both pancreatic cancer models studied, glucose is metabolized similarly in both primary and metastatic tumors even though glucose metabolism in the tumors differs from that observed in normal pancreas and liver.

To further study the metabolic relationship between primary pancreatic tumors, matched liver metastases, normal pancreas, and normal liver, we assessed overall metabolite levels in the tissues harvested from age-matched normal as well as tumor bearing mice. Unsupervised clustering of metabolites suggest that the metabolic profile of normal liver is distinct from the other samples (Fig 1M). Moreover, this type of analyses revealed minimal separation between the primary tumors, liver metastases, and the normal pancreas when the same data was analyzed using two different approaches, relative to normal liver (Fig. 1M-N). Of note, although we observe variability across samples, we do not find evidence of consistent changes in metabolites that distinguish primary and liver metastatic tumors from KPC mice (Fig. S3J).Taken together with the data assessing glucose fate, these data suggest that pancreatic tumors have a similar metabolic phenotype in both the primary site and in liver metastasis, and that the metabolic phenotype of a liver metastatic pancreatic tumor more closely resembles the tissue-of-origin than it does the metastatic tissue.

We next examined relative metabolite levels in cultured pancreatic cancer cells derived from primary tumors and liver metastases and found metabolite levels were similar across different independently derived paired primary and metastatic cells such that clustering based on metabolites did not uniformly segregate primary cells from liver metastatic cells (Fig. S4A). To examine whether nutrient utilization differs between primary- and liver metastasis-derived cancer cells in culture, we examined glucose metabolism by assessing the fate of U-^{13}C-glucose. Although some differences in glucose fate in culture were observed across different cells derived from primary and liver metastases, these differences were not consistent across multiple paired primary and liver metastatic lines from independent mice (Fig S4B-J). Taken together, these data argue that any metabolic differences that exist between primary and liver metastatic PDAC cells are not maintained in standard culture, and thus are not determined by stable genetic or epigenetic regulation of metabolism.

If the need to access a tissue environment with enough similarity to the primary tissue site is a barrier to metastasis, we reasoned that this may result in metastatic cancer cells retaining a preference to grow in the primary site. For instance, if a specific nutrient environment is needed to support the growth of tumors in either the primary and the metastatic sites, this would be better represented in the primary tissue and result in differences in the rate of tumor growth in different sites. To examine this possibility, we implanted cells derived from either primary tumors or matched liver metastases into the pancreas or liver, as well as into the flank as a neutral site that is commonly used to assess tumor growth in mice (Fig. 2A). In all cases we implanted the same number of

cells in each site, and after a fixed period of four weeks we assessed tumor weight where possible, or weight of the tumor bearing organ, as well as the wet tissue weight of the corresponding normal tissue from age-matched mice. We found that cancer cells from both primary and liver metastatic tumors were able to form tumors at all sites but observed a clear preference for cancer cells derived from both primary tumors and liver metastasis to form tumors in the pancreas, with much larger tumors forming in this organ than in the liver or flank (Fig. 2B, Fig. S5A-B). Interestingly, cancer cells formed tumors that grew to a similar size in each organ site regardless of whether the cells were derived from a primary or a liver-metastatic lesion. Tumors in each site were also histologically similar regardless of whether they were derived from a primary tumor or a liver metastasis (Fig. 2C, Fig. S5C). Proliferation of cells derived from primary or a liver-metastatic lesion, as determined by Ki-67 staining, was also similar in tumors at each site (Fig. 2D and Fig. S5D). Repeating this analysis with an independently derived matched primary and liver metastasis cell pair also showed a preference for both primary- and liver metastasis-derived cells to form large tumors in the pancreas (Fig S5E). These data argue that the pancreas better supports the growth of pancreatic cancer cells as tumors, even if those cancer cells are derived from liver metastasis.

To examine whether the tumor initiating capacity of primary- and liver metastasis-derived cells differ in different tissue locations, we implanted different numbers of either primary- or liver metastasis-derived pancreatic cancer cells into the pancreas or liver and determined the minimal number of cells competent to form tumors in each site. We found that both primary- and liver metastasis-derived cells have a similar tumor initiating

capacity at each site; however, more cells are needed to form a tumor in the liver than are needed to form tumors in the pancreas (Fig. 2E-F). These data further support the notion that pancreatic cancer cells retain a preference to grow in the primary site even if they are derived from a liver metastasis.

To assess whether PDAC lung metastatic cells also retain a preference to grow in the pancreas, we performed similar experiments using independently derived cells from matched primary, liver, and lung metastases arising in KPC mice (Fig. 2G). Cells derived from either liver metastases or lung metastases can form tumors in both the liver and lung; however, by far the largest tumors developed in the pancreas with the smallest tumors in the flank (Fig. 2H and Fig. S5F-L). These data argue cancer cells from metastasis retain a preference to grow in the primary site and may not adapt entirely to conditions in the metastatic site.

Propagation of cancer cells in metastatic sites has been used to select for cancer cells to grow in a particular tissue site and study metastasis, including assessment of metabolic differences between primary and metastatic tumors (*27*–*29*). Of note, these studies have largely examined the ability of selected cells to seed metastases when implanted in the primary site (*29*), and it remains unclear whether cells selected to seed metastatic sites also improve in their ability to grow in the different tissue sites once they arrive at that site. To answer this latter question, tumor cells derived from lung or liver metastases arising in KPC mice were propagated in vivo by three rounds of repeated implantation and passaging in the lung or liver respectively (Fig. 3A and Fig. S6A). Lung metastatic

cancer cells selected for in this manner efficiently formed lung tumors when injected via tail vein (Fig. S6B), and natural lung metastases developed in mice when these cells were implanted to form tumors in the pancreas (Fig. S6C). These same properties were present in the parental cells derived from a natural lung metastasis (Fig. S6B-C), which are otherwise infrequent in the KPC model (*19*). Propagating liver metastatic cancer cells as liver tumors in vivo resulted in more efficient tumor formation when implanted in the liver or when injected via tail vein (Fig. S6D-E). Of note, formation of liver nodules was not observed following tail vein injection of parental cells derived from liver metastases, arguing that in vivo passaging in the liver results in an increased ability to seed liver tumors.

Despite passaging cancer cells as tumors in the lung or liver, when their ability to form tumors in different tissue sites was quantitatively assessed over a defined time window, the in vivo selected cells still formed larger tumors in the pancreas (Fig. 3B-E and Fig. S6F). Again, cells derived from both liver and lung metastases were able to form tumors at all sites, with the largest tumors forming in the pancreas and the smallest in the flank. Notably, similar size tumors were observed at each site regardless of where the cells were derived and whether they were passaged previously as tumors in the liver or lung. These data support a model where the pancreatic cancer cells retain a preference to grow in the primary site, even when repeatedly passaged in a metastatic tissue site.

We next examined whether propagation of tumor cells in different tissues alters their metabolic phenotype. We first examined metabolites extracted from tumors that were

generated from cells derived from spontaneous lung metastases (P0) and from cells derived from in vivo selected lung metastases (P3) and compared those to metabolite levels extracted from primary pancreatic tumors as well as from age-matched normal lung or normal pancreas tissue. The small size of tumors that formed in the lung prevented assessment of metabolite levels when tumors are growing in that site, however we could assess metabolites extracted from the large tumors that formed in the pancreas to determine whether propagating cells in the lung stably selects for tumors with altered metabolism. We find that unsupervised clustering representation of the data as a heat map revealed that the pancreatic tumors derived from tumors that were generated from lung metastases, spontaneous or selected, metabolically cluster together with the primary tumor (Fig. 3F). When the same dataset was clustered using unsupervised K-means clustering, one *in vivo* adapted tumor clustered with the normal lung while the remaining tumor samples clustered together (Fig. 3G). These data suggest that passaging cancer cells as tumors in the lung, for the most part, does not select for stable alterations in metabolism that are retained when these cells are grown in the pancreas.

To assess whether a preference for cancer cells to form tumors in the pancreas is because this is the tissue of origin for the cancer cells considered, or the pancreatic microenvironment is more permissive to tumor growth, we asked whether cancer cells derived from different cancers also have a preference to grow in their primary tissue site compared to the pancreas. First, we considered primary lung adenocarcinoma cells derived from the *LSL-Kras*$^{G12D/+}$*; Trp53*$^{fl/fl}$*; Ad-Cre* mouse lung cancer model (*30*). Primary lung cancer cells did not grow well as tumors in the pancreas, yet these cells formed large

tumors in the lung of syngeneic mice (Fig. 4A). Of note, this preference to grow in the lung relative to the pancreas was the opposite of what we observed with pancreatic cancer lung metastasis-derived cells (Fig. S6G). Next, we performed a similar experiment using mouse hepatocellular carcinoma (HCC)-derived cells (*31*, *32*). These HCC cells were transplanted into the pancreas or liver of syngeneic mice, and tumor burden assessed after four weeks. While there was some variability between mice, HCC cells implanted into liver trended toward larger tumors relative to tumors that formed in the pancreas even after accounting for normal tissue weight (Fig. 4B and Fig. S6G). This preference for HCC-derived cells to grow in the liver relative to pancreas was again opposite of what was observed when compared directly to pancreatic cancer liver metastasis-derived cells (Fig. S6G). These data support that cancer cells retain a preference to grow in their tissue of origin relative to a metastatic site.

To further examine whether metastatic tumors retain the same metabolism as the primary site, we queried an available dataset to determine whether metabolic gene expression is conserved between primary, liver, and lung metastases in the KPC pancreatic cancer model (*22*). Analysis of metabolic genes from this single-cell RNA-seq (scRNA-seq) dataset revealed significant overlap between primary PDAC and liver metastases when all cells were analyzed (Fig. 4C). Of note, when the analysis was restricted to the most abundant clonal populations in the tumor samples in the dataset, despite evidence for heterogeneity in metabolic gene expression among cancer cells isolated from both the primary tumor and the metastases, the same heterogeneity in metabolic gene expression appeared to be present in cells derived from both the primary and metastatic sites (Fig.

4D-E, Fig. S7A). Interestingly, when barcoded cancer cells injected into the pancreas were subsequently traced across tissues, these clones cluster differently based on metabolic gene expression but do not segregate by tissue site (Fig. 4E, Fig. S7B). Thus, metabolic heterogeneity in these cells is driven by clonal relationships between cells and not the tissue environment where the cells are growing. That is, these data argue that despite heterogeneity in metabolic gene expression among pancreatic cancer cells isolated from each tissue site, and metabolic heterogeneity among cancer cell clones, there is not selection for a clone with a specific global change in metabolic gene expression to grow as a metastasis. Rather, these data suggest that PDAC cancer cells retain a similar metabolic gene expression program to support tumor growth regardless of site.

To assess whether these same findings are found in human pancreatic cancers, we analyzed expression of metabolic genes from available patient tumor-derived RNA-seq datasets (*33*, *34*). Consistent with tissue-of-origin having a stronger influence on metabolic gene expression than tissue site, we find significant overlap of metabolic gene expression between primary pancreatic tumors and liver metastatic pancreatic tumors, and that this metabolic gene expression is distinct from that observed in primary liver cancer and normal liver tissue (Fig. 4F and Fig. S7C-D). Notably, the human pancreatic cancer liver metastases that overlap most with primary liver cancer samples contain a higher degree of contamination with normal hepatocytes as determined by higher expression of hepatocyte markers (Fig. 4F and Fig. S7C-D).

These data do not rule out that some phenotypes are selected for to enable cancer cell growth in metastatic sites; however, the finding that metastases have a similar metabolic program as the primary tumor argues that cancer cells retain many aspects of a metabolic program that is defined by the tissue-of-origin even when exposed to a new metastatic tissue environment. Thus, despite evidence for specific metabolic adaptions that can promote growth of cancer in specific tissues (*13*, *35*–*39*), it appears that the metabolic plasticity of cancer cells is not as flexible as often assumed (*15*). Rather, it supports a model where a metabolic program derived from the cancer tissue-of-origin constrains where cancer cells can grow. A relative lack of metabolic plasticity may explain why chemotherapies that target metabolism remain effective in treating both primary and metastatic tumors, with patients selected for treatment based on the cancer tissue-of-origin. Moreover, this model may underlie, at least in part, why particular cancer types metastasize to stereotyped locations, as accessing a nutrient environment that is similar enough to the primary tumors may be necessary to support the metabolic program that is selected for within the primary tumor. Better understanding the impact of different tissue nutrient environments on proliferation of cancers arising in different sites will be important to further test this hypothesis and could inform the selection of treatment modalities for patients based on the pattern of metastasis for a given primary tumor.

References

1. D. Yang, M. G. Jones, S. Naranjo, W. M. Rideout, K. H. J. Min, R. Ho, W. Wu, J. M. Replogle, J. L. Page, J. J. Quinn, F. Horns, X. Qiu, M. Z. Chen, W. A. Freed-Pastor, C. S. McGinnis, D. M. Patterson, Z. J. Gartner, E. D. Chow, T. G. Bivona, M. M. Chan, N. Yosef, T. Jacks, J. S. Weissman, *bioRxiv*, in press, doi:10.1101/2021.10.12.464111.

2. T. Celià-Terrassa, Y. Kang, Distinctive properties of metastasis-initiating cells. *Genes Dev.* **30**, 892 (2016).

3. A. T. Boutin, W. T. Liao, M. Wang, S. S. Hwang, T. V. Karpinets, H. Cheung, G. C. Chu, S. Jiang, J. Hu, K. Chang, E. Vilar, X. Song, J. Zhang, S. Kopetz, A. Futreal, Y. A. Wang, L. N. Kwong, R. A. DePinho, Oncogenic Kras drives invasion and maintains metastases in colorectal cancer. *Genes Dev.* **31** (2017), doi:10.1101/gad.293449.116.

4. A. P. Makohon-Moore, M. Zhang, J. G. Reiter, I. Bozic, B. Allen, D. Kundu, K. Chatterjee, F. Wong, Y. Jiao, Z. A. Kohutek, J. Hong, M. Attiyeh, B. Javier, L. D. Wood, R. H. Hruban, M. A. Nowak, N. Papadopoulos, K. W. Kinzler, B. Vogelstein, C. A. Iacobuzio-Donahue, Limited heterogeneity of known driver gene mutations among the metastases of individual patients with pancreatic cancer. *Nat. Genet.* **49**, 358–366 (2017).

5. A. Muir, M. G. Vander Heiden, The nutrient environment affects therapy. *Science (80-.).* **360**, 962–963 (2018).

6. H. Ying, A. C. Kimmelman, C. A. Lyssiotis, S. Hua, G. C. Chu, E. Fletcher-sananikone, J. W. Locasale, J. Son, H. Zhang, J. L. Coloff, H. Yan, W. Wang, S.

Chen, A. Viale, H. Zheng, J. Paik, C. Lim, A. R. Guimaraes, E. S. Martin, J. Chang, A. F. Hezel, S. R. Perry, J. Hu, B. Gan, Y. Xiao, J. M. Asara, R. Weissleder, Y. A. Wang, L. Chin, L. C. Cantley, Oncogenic Kras Maintains Pancreatic Tumors through Regulation of Anabolic Glucose Metabolism. **4** (2010), doi:10.1016/j.cell.2012.01.058.

7. J. J. Kamphorst, M. Nofal, C. Commisso, S. R. Hackett, W. Lu, E. Grabocka, M. G. Vander Heiden, G. Miller, J. A. Drebin, D. Bar-Sagi, C. B. Thompson, J. D. Rabinowitz, Human pancreatic cancer tumors are nutrient poor and tumor cells actively scavenge extracellular protein. *Cancer Res.* (2015), doi:10.1158/0008-5472.CAN-14-2211.

8. C. Commisso, S. M. Davidson, R. G. Soydaner-Azeloglu, S. J. Parker, J. J. Kamphorst, S. Hackett, E. Grabocka, M. Nofal, J. A. Drebin, C. B. Thompson, J. D. Rabinowitz, C. M. Metallo, M. G. Vander Heiden, D. Bar-Sagi, Macropinocytosis of protein is an amino acid supply route in Ras-transformed cells. *Nature*. **497**, 633–7 (2013).

9. J. R. Mayers, M. E. Torrence, L. V. Danai, T. Papagiannakopoulos, S. M. Davidson, M. R. Bauer, A. N. Lau, B. W. Ji, P. D. Dixit, A. M. Hosios, A. Muir, C. R. Chin, E. Freinkman, T. Jacks, B. M. Wolpin, D. Vitkup, M. G. Vander Heiden, Tissue of origin dictates branched-chain amino acid metabolism in mutant Kras-driven cancers. *Science (80-.).* **353**, 1161–1165 (2016).

10. M. O. Yuneva, T. W. M. Fan, T. D. Allen, R. M. Higashi, D. V. Ferraris, T. Tsukamoto, J. M. Matés, F. J. Alonso, C. Wang, Y. Seo, X. Chen, J. M. Bishop, The metabolic profile of tumors depends on both the responsible genetic lesion

and tissue type. *Cell Metab.* **15**, 157–170 (2012).

11. M. R. Sullivan, L. V. Danai, C. A. Lewis, S. H. Chan, D. Y. Gui, T. Kunchok, E. A. Dennstedt, M. G. Vander Heiden, A. Muir, Quantification of microenvironmental metabolites in murine cancers reveals determinants of tumor nutrient availability. *Elife*. **8**, e44235 (2019).
12. B. I. Reinfeld, M. Z. Madden, M. M. Wolf, A. Chytil, J. E. Bader, A. R. Patterson, A. Sugiura, A. S. Cohen, A. Ali, B. T. Do, A. Muir, C. A. Lewis, R. A. Hongo, K. L. Young, R. E. Brown, V. M. Todd, T. Huffstater, A. Abraham, R. T. O'Neil, M. H. Wilson, F. Xin, M. N. Tantawy, W. D. Merryman, R. W. Johnson, C. S. Williams, E. F. Mason, F. M. Mason, K. E. Beckermann, M. G. Vander Heiden, H. C. Manning, J. C. Rathmell, W. K. Rathmell, Cell-programmed nutrient partitioning in the tumour microenvironment. *Nature*. **593**, 282–288 (2021).
13. G. B. Ferraro, A. Ali, A. Luengo, D. P. Kodack, A. Deik, K. L. Abbott, D. Bezwada, L. Blanc, B. Prideaux, X. Jin, J. M. Possada, J. Chen, C. R. Chin, Z. Amoozgar, R. Ferreira, I. X. Chen, K. Naxerova, C. Ng, A. M. Westermark, M. Duquette, S. Roberge, N. I. Lindeman, C. A. Lyssiotis, J. Nielsen, D. E. Housman, D. G. Duda, E. Brachtel, T. R. Golub, L. C. Cantley, J. M. Asara, S. M. Davidson, D. Fukumura, V. A. Dartois, C. B. Clish, R. K. Jain, M. G. Vander Heiden, Fatty acid synthesis is required for breast cancer brain metastasis. *Nat. Cancer*. **2**, 414–428 (2021).
14. T. Schild, V. Low, J. Blenis, A. P. Gomes, Unique Metabolic Adaptations Dictate Distal Organ-Specific Metastatic Colonization. *Cancer Cell*. **33** (2018), pp. 347–354.

15. C. Lehúede, F. Dupuy, R. Rabinovitch, R. G. Jones, P. M. Siegel, Metabolic plasticity as a determinant of tumor growth and metastasis. *Cancer Res.* **76** (2016), pp. 5201–5208.

16. E. Gaude, C. Frezza, Tissue-specific and convergent metabolic transformation of cancer correlates with metastatic potential and patient survival. *Nat. Commun.* **7**, 1–9 (2016).

17. J. Hu, J. W. Locasale, J. H. Bielas, J. O'Sullivan, K. Sheahan, L. C. Cantley, M. G. Vander Heiden, D. Vitkup, Heterogeneity of tumor-induced gene expression changes in the human metabolic network. *Nat. Biotechnol.* **31**, 522–529 (2013).

18. I. J. Fidler, The pathogenesis of cancer metastasis: The "seed and soil" hypothesis revisited. *Nat. Rev. Cancer*. **3** (2003), pp. 453–458.

19. S. R. Hingorani, L. Wang, A. S. Multani, C. Combs, T. B. Deramaudt, R. H. Hruban, A. K. Rustgi, S. Chang, D. A. Tuveson, Trp53R172H and KrasG12D cooperate to promote chromosomal instability and widely metastatic pancreatic ductal adenocarcinoma in mice. *Cancer Cell*. **7**, 469–483 (2005).

20. R. L. Siegel, K. D. Miller, H. E. Fuchs, A. Jemal, Cancer Statistics, 2021. *CA. Cancer J. Clin.* **71** (2021), doi:10.3322/caac.21654.

21. A. C. Obenauf, J. Massagué, Surviving at a Distance: Organ-Specific Metastasis. *Trends in Cancer*. **1** (2015), , doi:10.1016/j.trecan.2015.07.009.

22. K. P. Simeonov, C. N. Byrns, M. L. Clark, R. J. Norgard, B. Martin, B. Z. Stanger, J. Shendure, A. McKenna, C. J. Lengner, Single-cell lineage tracing of metastatic cancer reveals selection of hybrid EMT states. *Cancer Cell*. **39**, 1150-1162.e9 (2021).

23. I. Elia, G. Doglioni, S. M. Fendt, Metabolic Hallmarks of Metastasis Formation. *Trends Cell Biol.* **28** (2018), , doi:10.1016/j.tcb.2018.04.002.

24. A. N. Lau, Z. Li, L. V. Danai, A. M. Westermark, A. M. Darnell, R. Ferreira, V. Gocheva, S. Sivanand, E. C. Lien, K. M. Sapp, J. R. Mayers, G. Biffi, C. R. Chin, S. M. Davidson, D. A. Tuveson, T. Jacks, N. J. Matheson, O. Yilmaz, M. G. Vander Heiden, Dissecting cell-type-specific metabolism in pancreatic ductal adenocarcinoma. *Elife*. **9**, 1–35 (2020).

25. A. N. Ariston Gabriel, Q. Jiao, U. Yvette, X. Yang, S. A. Al-Ameri, L. Du, Y. shan Wang, C. Wang, Differences between KC and KPC pancreatic ductal adenocarcinoma mice models, in terms of their modeling biology and their clinical relevance. *Pancreatology*. **20** (2020), , doi:10.1016/j.pan.2019.11.006.

26. P. A. Pérez-Mancera, C. Guerra, M. Barbacid, D. A. Tuveson, What we have learned about pancreatic cancer from mouse models. *Gastroenterology*. **142** (2012), doi:10.1053/j.gastro.2012.03.002.

27. N. Yamaguchi, E. M. Weinberg, A. Nguyen, M. V. Liberti, H. Goodarzi, Y. Y. Janjigian, P. B. Paty, L. B. Saltz, T. P. Kingham, J. Loo, E. de Stanchina, S. F. Tavazoie, PCK1 and DHODH drive colorectal cancer liver metastatic colonization and hypoxic growth by promoting nucleotide synthesis. *Elife*. **8** (2019), doi:10.7554/eLife.52135.

28. A. J. Minn, G. P. Gupta, P. M. Siegel, P. D. Bos, W. Shu, D. D. Giri, A. Viale, A. B. Olshen, W. L. Gerald, J. Massagué, Genes that mediate breast cancer metastasis to lung. *Nature*. **436** (2005), doi:10.1038/nature03799.

29. P. D. Bos, X. H. F. Zhang, C. Nadal, W. Shu, R. R. Gomis, D. X. Nguyen, A. J.

Minn, M. J. Van De Vijver, W. L. Gerald, J. A. Foekens, J. Massagué, Genes that mediate breast cancer metastasis to the brain. *Nature*. **459** (2009), doi:10.1038/nature08021.

30. M. DuPage, A. L. Dooley, T. Jacks, Conditional mouse lung cancer models using adenoviral or lentiviral delivery of Cre recombinase. *Nat. Protoc.* **4**, 1064–1072 (2009).

31. T. Kapanadze, J. Gamrekelashvili, C. Ma, C. Chan, F. Zhao, S. Hewitt, L. Zender, V. Kapoor, D. W. Felsher, M. P. Manns, F. Korangy, T. F. Greten, Regulation of accumulation and function of myeloid derived suppressor cells in different murine models of hepatocellular carcinoma. *J. Hepatol.* **59** (2013), doi:10.1016/j.jhep.2013.06.010.

32. L. Zender, W. Xue, C. Cordón-Cardo, G. J. Hannon, R. Lucito, S. Powers, P. Flemming, M. S. Spector, S. W. Lowe, Generation and analysis of genetically defined liver carcinomas derived from bipotential liver progenitors. *Cold Spring Harb. Symp. Quant. Biol.* **70**, 251–261 (2005).

33. B. J. Raphael, R. H. Hruban, A. J. Aguirre, R. A. Moffitt, J. J. Yeh, C. Stewart, A. G. Robertson, A. D. Cherniack, M. Gupta, G. Getz, S. B. Gabriel, M. Meyerson, C. Cibulskis, S. S. Fei, T. Hinoue, H. Shen, P. W. Laird, S. Ling, Y. Lu, G. B. Mills, R. Akbani, P. Loher, E. R. Londin, I. Rigoutsos, A. G. Telonis, E. A. Gibb, A. Goldenberg, A. M. Mezlini, K. A. Hoadley, E. Collisson, E. Lander, B. A. Murray, J. Hess, M. Rosenberg, L. Bergelson, H. Zhang, J. Cho, G. Tiao, J. Kim, D. Livitz, I. Leshchiner, B. Reardon, E. Van Allen, A. Kamburov, R. Beroukhim, G. Saksena, S. E. Schumacher, M. S. Noble, D. I. Heiman, N. Gehlenborg, J. Kim,

M. S. Lawrence, V. Adsay, G. Petersen, D. Klimstra, N. Bardeesy, M. D. M. Leiserson, R. Bowlby, K. Kasaian, I. Birol, K. L. Mungall, S. Sadeghi, J. N. Weinstein, P. T. Spellman, Y. Liu, L. T. Amundadottir, J. Tepper, A. D. Singhi, R. Dhir, D. Paul, T. Smyrk, L. Zhang, P. Kim, J. Bowen, J. Frick, J. M. Gastier-Foster, M. Gerken, K. Lau, K. M. Leraas, T. M. Lichtenberg, N. C. Ramirez, J. Renkel, M. Sherman, L. Wise, P. Yena, E. Zmuda, J. Shih, A. Ally, M. Balasundaram, R. Carlsen, A. Chu, E. Chuah, A. Clarke, N. Dhalla, R. A. Holt, S. J. M. Jones, D. Lee, Y. Ma, M. A. Marra, M. Mayo, R. A. Moore, A. J. Mungall, J. E. Schein, P. Sipahimalani, A. Tam, N. Thiessen, K. Tse, T. Wong, D. Brooks, J. T. Auman, S. Balu, T. Bodenheimer, D. N. Hayes, A. P. Hoyle, S. R. Jefferys, C. D. Jones, S. Meng, P. A. Mieczkowski, L. E. Mose, C. M. Perou, A. H. Perou, J. Roach, Y. Shi, J. V. Simons, T. Skelly, M. G. Soloway, D. Tan, U. Veluvolu, J. S. Parker, M. D. Wilkerson, A. Korkut, Y. Senbabaoglu, P. Burch, R. McWilliams, K. Chaffee, A. Oberg, W. Zhang, M. C. Gingras, D. A. Wheeler, L. Xi, M. Albert, J. Bartlett, H. Sekhon, Y. Stephen, Z. Howard, M. Judy, A. Breggia, R. T. Shroff, S. Chudamani, J. Liu, L. Lolla, R. Naresh, T. Pihl, Q. Sun, Y. Wan, Y. Wu, S. Jennifer, K. Roggin, K. F. Becker, M. Behera, J. Bennett, L. Boice, E. Burks, C. G. Carlotti Junior, J. Chabot, D. Pretti da Cunha Tirapelli, J. Sebastião dos Santos, M. Dubina, J. Eschbacher, M. Huang, L. Huelsenbeck-Dill, R. Jenkins, A. Karpov, R. Kemp, V. Lyadov, S. Maithel, G. Manikhas, E. Montgomery, H. Noushmehr, A. Osunkoya, T. Owonikoko, O. Paklina, O. Potapova, S. Ramalingam, W. K. Rathmell, K. Rieger-Christ, C. Saller, G. Setdikova, A. Shabunin, G. Sica, T. Su, T. Sullivan, P. Swanson, K. Tarvin, M. Tavobilov, L. B. Thorne, S. Urbanski, O.

Voronina, T. Wang, D. Crain, E. Curley, J. Gardner, D. Mallery, S. Morris, J. Paulauskis, R. Penny, C. Shelton, T. Shelton, K. P. Janssen, O. Bathe, N. Bahary, J. Slotta-Huspenina, A. Johns, H. Hibshoosh, R. F. Hwang, A. Sepulveda, A. Radenbaugh, S. B. Baylin, M. Berrios, M. S. Bootwalla, A. Holbrook, P. H. Lai, D. T. Maglinte, S. Mahurkar, T. J. Triche, D. J. Van Den Berg, D. J. Weisenberger, L. Chin, R. Kucherlapati, M. Kucherlapati, A. Pantazi, P. Park, G. Saksena, D. Voet, P. Lin, S. Frazer, T. Defreitas, S. Meier, L. Chin, S. Y. Kwon, Y. H. Kim, S. J. Park, S. S. Han, S. H. Kim, H. Kim, E. Furth, M. Tempero, C. Sander, A. Biankin, D. Chang, P. Bailey, A. Gill, J. Kench, S. Grimmond, A. Johns, A. P. Cancer Genome Initiative (APGI, R. Postier, R. Zuna, H. Sicotte, J. A. Demchok, M. L. Ferguson, C. M. Hutter, K. R. Mills Shaw, M. Sheth, H. J. Sofia, R. Tarnuzzer, Z. Wang, L. Yang, J. (Julia) Zhang, I. Felau, J. C. Zenklusen, Integrated Genomic Characterization of Pancreatic Ductal Adenocarcinoma. *Cancer Cell*. **32**, 185-203.e13 (2017).

34. A. J. Aguirre, J. A. Nowak, N. D. Camarda, R. A. Moffi tt, A. A. Ghazani, M. Hazar-Rethinam, S. Raghavan, J. Kim, L. K. Brais, D. Ragon, M. W. Welch, E. Reilly, D. McCabe, L. Marini, K. Anderka, K. Helvie, N. Oliver, A. Babic, A. Da Silva, B. Nadres, E. E. Van Seventer, H. A. Shahzade, J. P. St Pierre, K. P. Burke, T. Clancy, J. M. Cleary, L. A. Doyle, K. Jajoo, N. J. McCleary, J. A. Meyerhardt, J. E. Murphy, K. Ng, A. K. Patel, K. Perez, M. H. Rosenthal, D. A. Rubinson, M. Ryou, G. I. Shapiro, E. Sicinska, S. G. Silverman, R. J. Nagy, R. B. Lanman, D. Knoerzer, D. J. Welsch, M. B. Yurgelun, C. S. Fuchs, L. A. Garraway, G. Getz, J. L. Hornick, B. E. Johnson, M. H. Kulke, R. J. Mayer, J. W. Miller, P. B.

Shyn, D. A. Tuveson, N. Wagle, J. Jen Yeh, W. C. Hahn, R. B. Corcoran, S. L. Carter, B. M. Wolpin, C. Authors, Real-time Genomic Characterization of Advanced Pancreatic Cancer to Enable Precision Medicine. *CANCER Discov.* **8**, 1097 (2018).

35. Z. T. Schug, B. Peck, D. T. Jones, Q. Zhang, S. Grosskurth, I. S. Alam, L. M. Goodwin, E. Smethurst, S. Mason, K. Blyth, L. McGarry, D. James, E. Shanks, G. Kalna, R. E. Saunders, M. Jiang, M. Howell, F. Lassailly, M. Z. Thin, B. Spencer-Dene, G. Stamp, N. J. F. van den Broek, G. Mackay, V. Bulusu, J. J. Kamphorst, S. Tardito, D. Strachan, A. L. Harris, E. O. Aboagye, S. E. Critchlow, M. J. O. Wakelam, A. Schulze, E. Gottlieb, Acetyl-CoA synthetase 2 promotes acetate utilization and maintains cancer cell growth under metabolic stress. *Cancer Cell*. **27**, 57–71 (2015).

36. I. Elia, M. Rossi, S. Stegen, D. Broekaert, G. Doglioni, M. van Gorsel, R. Boon, C. Escalona-Noguero, S. Torrekens, C. Verfaillie, E. Verbeken, G. Carmeliet, S. M. Fendt, Breast cancer cells rely on environmental pyruvate to shape the metastatic niche. *Nature*. **568**, 117–121 (2019).

37. G. Rinaldi, E. Pranzini, J. Van Elsen, D. Broekaert, C. M. Funk, M. Planque, G. Doglioni, P. Altea-Manzano, M. Rossi, V. Geldhof, S. T. Teoh, C. Ross, K. W. Hunter, S. Y. Lunt, T. G. P. Grünewald, S. M. Fendt, In Vivo Evidence for Serine Biosynthesis-Defined Sensitivity of Lung Metastasis, but Not of Primary Breast Tumors, to mTORC1 Inhibition. *Mol. Cell*. **81**, 386-397.e7 (2021).

38. I. Elia, D. Broekaert, S. Christen, R. Boon, E. Radaelli, M. F. Orth, C. Verfaillie, T. G. P. Grünewald, S. M. Fendt, Proline metabolism supports metastasis formation

and could be inhibited to selectively target metastasizing cancer cells. *Nat. Commun.* **8**, 1–11 (2017).

39. Y. Chi, J. Remsik, V. Kiseliovas, C. Derderian, U. Sener, M. Alghader, F. Saadeh, K. Nikishina, T. Bale, C. Iacobuzio-Donahue, T. Thomas, D. Pe'er, L. Mazutis, A. Boire, Cancer cells deploy lipocalin-2 to collect limiting iron in leptomeningeal metastasis. *Science (80-.).* **369**, 276–282 (2020).

40. N. Bardeesy, K. H. Cheng, J. H. Berger, G. C. Chu, J. Pahler, P. Olson, A. F. Hezel, J. Horner, G. Y. Lauwers, D. Hanahan, R. A. DePinho, Smad4 is dispensable for normal pancreas development yet critical in progression and tumor biology of pancreas cancer. *Genes Dev.* **20**, 3130–3146 (2006).

41. S. F. Boj, C. Il Hwang, L. A. Baker, I. I. C. Chio, D. D. Engle, V. Corbo, M. Jager, M. Ponz-Sarvise, H. Tiriac, M. S. Spector, A. Gracanin, T. Oni, K. H. Yu, R. Van Boxtel, M. Huch, K. D. Rivera, J. P. Wilson, M. E. Feigin, D. Öhlund, A. Handly-Santana, C. M. Ardito-Abraham, M. Ludwig, E. Elyada, B. Alagesan, G. Biffi, G. N. Yordanov, B. Delcuze, B. Creighton, K. Wright, Y. Park, F. H. M. Morsink, I. Q. Molenaar, I. H. Borel Rinkes, E. Cuppen, Y. Hao, Y. Jin, I. J. Nijman, C. Iacobuzio-Donahue, S. D. Leach, D. J. Pappin, M. Hammell, D. S. Klimstra, O. Basturk, R. H. Hruban, G. J. Offerhaus, R. G. J. Vries, H. Clevers, D. A. Tuveson, Organoid models of human and mouse ductal pancreatic cancer. *Cell*. **160**, 324–338 (2015).

42. V. Gocheva, A. Naba, A. Bhutkar, T. Guardia, K. M. Miller, C. M. C. Li, T. L. Dayton, F. J. Sanchez-Rivera, C. Kim-Kiselak, N. Jailkhani, M. M. Winslow, A. Del Rosario, R. O. Hynes, T. Jacks, Quantitative proteomics identify Tenascin-C as a

promoter of lung cancer progression and contributor to a signature prognostic of patient survival. *Proc. Natl. Acad. Sci. U. S. A.* **114** (2017), doi:10.1073/pnas.1707054114.

43. S. M. Davidson, T. Papagiannakopoulos, B. A. Olenchock, J. E. Heyman, M. A. Keibler, A. Luengo, M. R. Bauer, A. K. Jha, J. P. O'Brien, K. A. Pierce, D. Y. Gui, L. B. Sullivan, T. M. Wasylenko, L. Subbaraj, C. R. Chin, G. Stephanopolous, B. T. Mott, T. Jacks, C. B. Clish, M. G. Van Der Heiden, Environment impacts the metabolic dependencies of ras-driven non-small cell lung cancer. *Cell Metab.* **23**, 517–528 (2016).

44. C. A. Lewis, S. J. Parker, B. P. Fiske, D. McCloskey, D. Y. Gui, C. R. Green, N. I. Vokes, A. M. Feist, M. G. Vander Heiden, C. M. Metallo, Tracing Compartmentalized NADPH Metabolism in the Cytosol and Mitochondria of Mammalian Cells. *Mol. Cell*. **55**, 253–263 (2014).

Acknowledgements: We would like to thank the MIT Division of Comparative Medicine (DCM) staff and Kylee Pait for help with colony maintenance and animal care, and the Koch Institute Swanson Biotechnology Center for technical support, specifically the Hope Babette Tang Histology Core, and the Flow Cytometry Core. We would also like to thank all members of the Vander Heiden lab for helpful discussions and feedback and note that some schematic images were created using BioRender.com.

Funding: S.S. acknowledges support from the Damon Runyon Cancer Research Foundation (DRG-2367-19). L.V.D. was supported by F32CA21042. A.N.L. was a Robert

Black Fellow of the Damon Runyon Cancer Research Foundation (DRG-2241-15) and was supported by K99CA234221. A.M.D. acknowledges support from a Jane Coffin Childs Postdoctoral Fellowship. M.G.V.H. acknowledges support from the Lustgarten Foundation, a Faculty Scholar grant from the Howard Hughes Medical Institute, the MIT Center for Precision Cancer Medicine, the Ludwig Center at MIT, the Emerald Foundation, Stand Up To Cancer, and the NCI (R35CA242379, R01CA201276, R01CA259253, P30CA14051).

Author contributions: S.S.: conceptualization, investigation, visualization, methodology, writing- original draft, writing review and editing. Y.G., P.S.W., S.Y.V., K.M.T., L.V.D., B.T.D., K.C., T.K., A.N.L., A.M.D., C.A.L.: methodology, investigation, writing- review and editing. S.M. and D.G.D.: methodology. D.V., B.M.W., A.K.S.: supervision, M.G.V.H.: conceptualization, supervision, visualization, funding acquisition, project administration, methodology, writing-original draft, writing- review and editing.

Competing interests: M.G.V.H. is a scientific advisor for Agios Pharmaceuticals, iTeos Therapeutics, Faeth Therapeutics, Sage Therapeutics, and Auron Therapeutics. A.N.L.: Present address: Pfizer Inc., 1 Portland St., Cambridge, MA, 02139, USA. All other authors declare no competing interests.

Data and materials availability: All data are presented or provided in the supplementary materials.

Materials and Methods

Animal studies

All studies were approved by the MIT committee on Animal Care under protocol number #0119-001-22. For autochthonous models, *Kras$^{G12D/+}$; Trp53$^{R172H/+}$; Pdx1-Cre* (KPC) (*40*) and *Kras$^{G12D/+}$; Trp53$^{R172H/+}$; Pdx1-Cre; LSL-tdTomato* (KPCT) (*19*) mice from a mixed 129/Sv and C57Bl6/J background as well as pure C57Bl6/J genetic background were used. Both male and female pure C57Bl6/J mice were used for all transplantation experiments. For metabolomics experiments normal tissue was isolated from age-matched 6-month-old mice while tumors and paired liver metastases were isolated from the same 6–8-month-old animals. Animals were housed under 12-hour light and 12-hour dark cycle, and co-housed with littermates with ad libitum access to water and food, except immediately following surgical procedures.

Tumor transplantation

Both male and female animals were used for these studies. For subcutaneous, pancreatic, or intrahepatic transplantation studies, C57B16/J mice aged approximately 6-8 weeks were injected with 100,000 cells PDAC cells derived from primary or metastatic tumors arising in KPC or KPCT mice at the indicated site. To deliver cancer cells to the

lung, 100,000 cells were injected via tail vein. Mice were euthanized 4 weeks post injection of tumor cells or at signs of animal distress. All mice within the same experimental group were euthanized at the same time point.

For limiting dilution studies, mice were injected with the indicated number of cells and monitored twice a week for signs of tumor burden. The tumor initiating capacity was calculated using ELDA software (http://bioinf.wehi.edu.au/software/elda/). At least 3 mice were included for each condition.

For cell competition experiments, pancreatic cancer cells derived from primary or liver metastatic tumors were engineered to express either mCherry or GFP and mixed in equal numbers. Pre-injection representation was confirmed using flow cytometry (BD LSR-II). 100,000 cells containing the mixed population were injected into the pancreas, liver, or subcutaneously, and after tumors formed, they were excised, digested, and analyzed by flow cytometry to determine relative representation in the tumor.

For metastatic stie adaptation experiments, cells from liver and lung metastatic tumors arising in the KPC model were isolated and cultured for less than 10 population doublings. Cells from the lung metastases were then transplanted into the lung via tail vein injection. Resulting tumors were dissociated and re-transplanted into secondary recipient mice without *in vitro* propagation. This process was repeated three times. A similar approach was taken with the liver metastases where cells were propagated in the liver. Mice were euthanized at different time points based on established and approved criteria, and

following the last round of *in vivo* selection, tumors were dissociated and cultured for less than 5 population doublings before use in transplantation experiments (P0 refers to the parental cells (prior to *in vivo* adaptation); P3 refers to the tumor and tumor cells derived from three round of *in vivo* adaptation).

Cell isolation and cell culture

Cells were isolated from primary and metastatic mouse pancreatic tumors as described previously (*41*). Briefly, tumors were exteriorized, minced, and digested with collagenase XI (Sigma C9407) and dispase II (Roche 04942078001) and plated in DMEM. RIL-175 mouse hepatocellular carcinoma cells were derived from hepatic tumors established in C57BL/6 mice as previously described (*31*). Lung adenocarcinoma cells were obtained from the *LSL*-Kras(G12D); *Trp53*$^{fl/fl}$*; Ad-Cre* mouse lung cancer model as previously described (*42*). Cells were cultured in DMEM (Corning 10-013-CV) supplemented with 10% heat inactivated fetal bovine serum. Penicillin-streptomycin was added only at the time of cell isolation from mice. Cells were regularly tested for mycoplasma contamination using the MycoAlert Plus kit (Lonza).

Isotope labeling experiments in cultured cells

Cells were plated in 6-well plates, and the next day cells were washed three times with warm PBS, and DMEM without glucose and pyruvate supplemented with 10% dialyzed FBS and 10 mM U-^{13}C-glucose (Cambridge Isotope Laboratories) was added for 24 hours prior to metabolite extraction.

Glucose infusions

Infusion of U-^{13}C glucose (Cambridge Isotope Laboratories) into control or tumor bearing mice was performed as previously described (*24*, *43*). Three-weeks after implantation of cancer cells, animals underwent surgical catheter implantation in the jugular vein 3-4 days prior to labeled glucose infusion. Mice were fasted for 4 hours prior to starting the infusion and animals remained conscious and mobile for the duration of the infusion. Labeled glucose was delivered at a rate of 0.4 mg/min for 6 hours, and then plasma and tumor tissue was isolated and flash frozen for analysis by mass spectrometry.

Metabolite Extraction

To analyze glucose in plasma, 10 μL of plasma was extracted with 100% methanol and dried down with nitrogen and derivatized with 50 μL of 2 wt% hydroxylamine hydrochloride (2% Hox) in pyridine followed by incubation at 90°C for 60 min. 100 μL of propionic anhydride was added, and samples were incubated at 60°C for 30 min, followed by evaporation under nitrogen at room temperature overnight. The next day, dried samples were dissolved in 100 μL of ethyl acetate and transferred to glass vials for analysis by GC-MS.

For tissue metabolite analysis, the harvested tissues were rinsed briefly in ice-cold blood blank saline and flash frozen in liquid nitrogen. Frozen tissues were then ground into powder using a pre-chilled mortar and pestle. The tissue powder was then weighed into pre-chilled tubes and extracted with methanol (containing 500 nM each of 17 isotopically labeled ^{13}C/^{15}N amino acids (Cambridge Isotope Laboratories, Inc.)): chloroform: water

(6:3:4 v/v/v), vortexed for 10 min and centrifuged for 10 min at maximum speed. Polar metabolites were transferred to Eppendorf tubes, dried under nitrogen gas, and resuspended in different volumes of water containing labeled non-standard amino acid mix (Cambridge Isotope Laboratories, MSK-NCAA-1) to account for differences in starting tissue weight.

For cultured cells, cells were seeded at 30,000 cells/well in a 6 well dish in 2 mL of medium and incubated for 72 hour, or 100,000 cells were plated and incubated overnight. Media was aspirated from cells and then washed rapidly in ice cold bank saline followed by addition of 500 mL ice-cold 80% methanol in water containing 500 nM each of 17 isotopically labeled $^{13}C/^{15}N$ amino acids (Cambridge Isotope Laboratories). Alternatively, for metabolite analysis by GC-MS, cells were extracted in equal parts 80% methanol (containing 2.5 ng/mL norvaline internal standard) and chloroform. Samples were vortexed 10 min at 4°C and spun at 16,000 xg for 10 min at 4°C. Equal volume of the polar fraction was transferred to a new tube and dried down under nitrogen and frozen at -80°C prior to analysis by mass spectrometry.

Gas chromatography-mass spectrometry

GC-MS was used to analyze metabolites as previously described (*44*). Briefly, dried metabolite extracts were dissolved in 16 mL methoxamine (MOX) reagent (ThermoFisher TS-45950) and incubated at 37°C for 90 min. 20 mL N–methyl–N–(tert–butyldimethylsilyl)trifluor-oacetamide + 1% tert–Butyldimethylchlorosilane (Sigma 375934) was added to the sample and incubated at 60°C for 1 hour. Samples were

centrifuged for 5 min and 20 mL of the derivatized sample was transferred to GC vial for analysis using a DB-35MS column (Agilent Technologies 122-3832) installed in an Agilent 7890 gas chromatograph coupled to an Agilent 5975C mass spectrometer. The helium carrier gas was used at a constant flow rate of 1.2mL/min. One microliter of the sample was injected at 270°C. After injection, the GC oven was held at 100°C for 1 min, increased to 300°C at 3.5°C/min. The oven was then ramped up to 320°C at 20°C/min and held for 5 min at 320°C. The MS system operated under electron impact ionization at 70 eV and the MS source and quadrupole was held at 230°C and 150°C, respectively. The detector was used in scanning mode and the scanned ion range was 100-650 m/z. Total ion counts were determined by integrating appropriate ion fragments for each metabolite using El-Maven software (Elucidata).

Liquid chromatography-mass spectrometry

Metabolite profiling was conducted on a QExactive bench top orbitrap mass spectrometer equipped with an Ion Max source and a HESI II probe, which was coupled to a Dionex UltiMate 3000 HPLC system (Thermo Fisher Scientific, San Jose, CA). External mass calibration was performed using the standard calibration mixture every 7 days. Typically, samples were reconstituted in 50 uL water and 2 uL were injected onto a SeQuant® ZIC®-pHILIC 150 x 2.1 mm analytical column equipped with a 2.1 x 20 mm guard column (both 5 mm particle size; EMD Millipore). Buffer A was 20 mM ammonium carbonate, 0.1% ammonium hydroxide; Buffer B was acetonitrile. The column oven and autosampler tray were held at 25◦C and 4◦C, respectively. The chromatographic gradient was run at a flow rate of 0.150 mL/min as follows: 0-20 min: linear gradient from 80-20% B; 20-20.5

min: linear gradient form 20-80% B; 20.5-28 min: hold at 80% B. The mass spectrometer was operated in full-scan, polarity-switching mode, with the spray voltage set to 3.0 kV, the heated capillary held at 275◦C, and the HESI probe held at 350◦C. The sheath gas flow was set to 40 units, the auxiliary gas flow was set to 15 units, and the sweep gas flow was set to 1 unit. MS data acquisition was performed in a range of *m/z* = 70–1000, with the resolution set at 70,000, the AGC target at $1x10^6$, and the maximum injection time at 20 msec. Relative quantitation of polar metabolites was performed with TraceFinder™ 4.1 (Thermo Fisher Scientific) using a 5-ppm mass tolerance and referencing an in-house library of chemical standards. Data were filtered according to predetermined QC metrics: CV of pools <25%; R of linear dilution series <0.975. Data was normalized to cell number from a separately plated set of samples collected at the time of metabolite extraction.

For untargeted metabolomics, data were acquired as described above, with $ddMS^2$ data collected on pooled samples using a Top-10 method, with stepped collision energies of 15, 30 and 45 V. The resolution was set at 17,500, the AGC target was $2x10^5$, the max IT was 100 ms, and the isolation window was set at 1.0 m/z. Data were analyzed using Compound Discoverer 3.1 (Thermo Fisher Scientific) and by including an in-house mass-list. P-values were adjusted according to the Benjamini-Hochberg method.

Cell proliferation

30,000 cells were plated in a 6 well plate in 2 mL of DMEM with 10% FBS and cultured for at least 12 h. Cells were washed once, and media was replaced with fresh DMEM at

the time of cell counting on day 0 using a Cellometer Auto T4 Plus Cell Counter (Nexcelom Bioscience). Cells counted again 3 days later, and doublings per day was calculated using the formula: Proliferation rate (Doublings/day) = Log_2(Final cell count (day 3)/initial cell count (day 0))/3 (days).

Flow cytometry

Tumors were dissected, minced, and digested at 37°C for 30 min with 1 mg/mL Collagenase I (Worthington Biochemical, LS004194), 3 mg/mL Dispase II (Roche, 04942078001), and 0.1 mg/mL DNase I (Sigma, D4527) in 5 mL PBS. After 30 min, cells were incubated with EDTA to 10 mM at room temperature for 5 min. Cells were filtered through a 70 mm cell strainer, washed twice in PBS, and cells resuspended in flow cytometry staining buffer (Thermo Fischer, 00-4222-57) for fluorescent protein expression analysis on a BD-LSR II flow cytometer.

Immunohistochemistry

Tissue was fixed in formalin for at least 24 h. Sections from formalin fixed paraffin embedded tissues were stained using antibodies against mCherry (1:500 dilution; Novus Biologicals: NBP1-96752), GFP (1:250 dilution; Novus Biologicals: NB600-308), pan-cytokeratin (1:500 dilution; abcam: ab133496), or Ki67 (1:250 dilution; Novus Biologicals: NB110-89717). Antibodies were diluted in 10% normal goat serum diluted 1:2 (Thermo Fischer: 50062Z) in PBS-T.

Histology and image analysis

Histology sections were scanned using Aperio Digital Scanning and imported into Aperio eSlide Manager. Image analysis was done using Fiji software. Tumor area and total area was calculated for all the sections and the net tumor area was calculated by dividing the tumor area by the total area. The number of nodules in the lung was calculated manually.

RNA-sequencing analysis of mouse tumors

Metabolic gene expression analysis of mouse tumors was done using pancreatic tumors single cell RNA-sequencing data from a published source (*22*). PCA plots depict analysis of metabolic genes from entire cell populations. For mouse single-cell RNA-seq data analysis, after normalizing to total counts, metabolic genes were analyzed from primary, liver, or lung metastases and UMAP plots for the most abundant samples were generated using scanpy version 1.8.0 to determine overlap between gene expression across tissue sites. For single cell analysis, lineage tracing of the most represented cell clones from the study permitted analysis of individual clonal populations and UMAP plots depict overlap between gene expression across overrepresented clones within the tumor across different tissue sites. Pearson correlation was also found between pairs of single cells using the scores for the top 20 PCs.

RNA-sequencing analysis of human tumors

FASTQs for bulk RNA expression profiles were downloaded from the relevant repository (TCGA, https://toil.xenahubs.net; Metastatic PDAC, dbGaP Study Accession phs001652.v1.p1) and all data were processed using the same pipeline. Briefly, each sample's sequences were marked for duplicates and then mapped to hg38 using STAR.

After running QC checks using RNAseqQC, gene-level count matrices were generated using RSEM. Instructions to run the pipeline are given in the Broad CCLE github repository https://github.com/broadinstitute/ccle_processing. Length-normalized values (TPM) were then transformed according to log2(TPM+1) for downstream analysis. We then scaled and centered the entire dataset to allow relative comparisons across sample types (Normal Liver, HCC, PDAC, and metastatic PDAC).

We tested whether metastatic PDAC more closely resembles the metabolic state of the primary site (pancreas) or the dominant metastatic tissue of residence (liver) and used normal liver and hepatocellular carcinoma (HCC) profiles as relevant comparators. To do this, we trimmed the expression data to 3,240 metabolically associated genes using a literature-curated list. We then performed a cross-correlational analysis (Pearson's *r*) across all samples and separated this matrix by study after clustering (Ward's method). We then generated similarity scores for each metastatic sample (n = 49) by computing their average Pearson's *r* to either primary PDAC, HCC, or normal liver samples.

Statistical Analysis

Results are represented as mean +/- standard deviation unless otherwise specified. Statistical analysis was performed using GraphPad Prism Software (Version 9.1.1). The statistical significance between two groups were calculated using unpaired two-tailed student *t* test where noted.

Figure legends

Fig. 1. Primary and metastatic pancreatic tumors have similar metabolic phenotypes. (**A)** The same cancer cells isolated from a primary pancreatic tumor arising in a KPC mouse were engineered to express either mCherry or GFP and combined in equal numbers prior to implantation into different tissue sites in mice. Flow cytometry confirming that approximately equal representation of each labeled cancer cell population is present in the mixed population. (**B-D**) Representation of mCherry and GFP labeled cells in tumors derived from injection of the mixed population shown in A into the pancreas (B), liver (C), or subcutaneous space (D). (**E**-**L**) Paired pancreatic cancer cells derived from primary tumors or liver metastases arising in the KPC mouse model were implanted into the pancreas or liver, respectively, and the resulting tumor-bearing mice were infused for 6 hours with U-^{13}C glucose at 0.4 mg/min to assess glucose fate in tumors growing in each site. Fractional labeling of the indicated metabolites as determined by GC-MS is shown. Data are from 3-4 mice per group. Mean +/- stdev. (**M-N**) Relative metabolite levels in autochthonous paired primary pancreatic cancer and liver metastases arising in KPC mice were assessed by LC-MS. Metabolite levels were also measured for normal pancreas and liver tissue from age-matched wild-type mice. The metabolite data for each sample is clustered in two different ways: Unsupervised clustering represented as a heatmap (M) or K-means unsupervised clustering (N); 6 mice were used for the normal tissue analysis and 4 mice were used for the paired primary tumor and metastasis analysis.

Fig. 2. Pancreatic cancer cells derived from both the primary tumor and from metastatic sites generate tumors that grow fastest in the pancreas. (**A**) Schematic depicting transplantation experiments to quantitatively assess pancreatic cancer cell proliferation in different tissue sites. (**B**) Equal numbers of cancer cells isolated from primary pancreatic tumors or paired liver metastases arising in the KPC mouse model were implanted into the pancreas, liver, or subcutaneous space, and resulting tumor size assessed after four weeks. Tissue site indicates the site where cells were implanted, and cells injected indicates whether the cells injected were derived from a primary tumor or liver metastasis (liver met). Relative weights of tumor and associated normal tissue compared with normal tissue of age-matched mice, or tumor weight in the subcutaneous flank, is shown. n=3-5 per group. Male mice were used for all the comparisons. Mean+/- stdev is shown. * $p < 0.05$; n.s. – not significant. (**C**) Hematoxylin and Eosin (H&E) staining of tissue sections involving tumors arising from primary pancreas or liver metastatic cancer cells implanted in the pancreas or liver as indicated. The boundary between normal tissue and tumor is indicated. Scale bar- 3700 μm (lower magnification; 0.3x); 500 μm (higher magnification; 2x) (**D**) The percent of cells that stain positive for Ki67 by immunohistochemistry was quantified in tissue sections from tumors arising from primary pancreatic cancer or liver metastatic cells implanted into the pancreas or liver as indicated. Data from 4-5 mice is shown; Ki67 percentage = number of positive stained cell in each image field was divided by the total number of cells in the same field x 100. One representative field per tumor was analyzed (**E-F**) The indicated number of cancer cells derived from a primary pancreatic tumor (P) or liver metastases (M) were implanted into either the pancreas (E) or the liver (F), and animals follow to determine if a tumor

formed as well as how long mice with tumors survived post-implantation; male mice were used for all the conditions. The number of mice with tumors is shown, with the total number of mice injected for each number of cells indicated in parentheses. These data were also used to calculate an approximate tumor initiating capacity (TIC) for primary- and metastasis-derived cells at each tissue site: Pancreas, primary (1/63.4), liver met (1/99.2), p-value = 0.531; Liver, primary (1/417), liver met (1/2005), p-value= 0.106. (**G**) Schematic depicting transplantation experiments to quantitatively assess pancreatic cancer cell proliferation in different tissue sites. (**H**) Equal numbers of cancer cells isolated from primary pancreatic tumors or paired liver or lung metastases arising in the KPC mouse model were implanted into the pancreas, liver, lung (via tail vein), or subcutaneous space, and resulting tumor size assessed after four weeks. As in B, relative weights of tumor and associated normal tissue compared with normal tissue of age-matched mice, or tumor weight in the subcutaneous flank, is shown, n=3-5 per group, Mean+/- stdev is shown. * $p < 0.05$, ** $p< 0.05$, and **** $p < 0.0001$; n.s. – not significant.

Fig. 3. Pancreatic cancer cells retain metabolic phenotypes found in the primary tumor even when repeatedly passaged in a metastatic site. (**A**) Schematic depicting propagation of lung and liver pancreatic cancer metastases arising in KPC mice by implantation into the lung or liver to form tumors three times prior to use in transplantation experiments to quantitatively assess proliferation and metabolic phenotypes in different tissue sites. (**B-E**) Equal numbers of cancer cells isolated from primary pancreatic tumors, paired liver, or lung metastases (P0), or liver or lung metastatic cancer cells that were passaged in the liver or lung as described in A (P3) were implanted into the pancreas, liver, lung (via tail

vein), or subcutaneous space, and resulting tumor size assessed after 3 weeks. Relative weights of tumor and associated normal tissue compared with normal tissue of age-matched mice, or tumor weight in the subcutaneous flank, is shown. Mean+/- stdev; n.s.- not significant, ** p<0.005; *p <0.05; n=3-5 mice per group. (**F-G**) Relative metabolite levels arising in tumors from primary, P0 and P3 lung metastases cells implanted in the pancreas (primary) or lung were assessed by LC-MS. Metabolite levels were also measured for normal pancreas and liver tissue from age-matched wild-type mice. The metabolite data for each sample is clustered in two different ways: Unsupervised clustering represented as a heatmap (F) or K-means unsupervised clustering (G).

Fig. 4. Tissue-of-origin influences the metabolism and tissue site preference for metastatic tumor growth. (**A**) Equal numbers of lung adenocarcinoma cells derived from the *LSL-Kras$^{G12D/+}$; Trp53$^{fl/fl}$; Ad-Cre* mouse model were implanted into the pancreas or delivered to the lung and resulting tumor size assessed after four weeks. Relative weights of tumor and associated normal tissue compared with normal tissue from age-matched mice is shown. Mean+/- stdev; * p<0.05, **** p<0.0001; n=3-5 mice per group macroscopic images at the time of tissue harvest are also shown. (**B**) Equal numbers of RIL-176 hepatocellular carcinoma (HCC) cells were implanted into the pancreas or the liver and resulting tumor size assessed after four weeks. Relative weights of tumor and associated normal tissue compared with normal tissue from age-matched mice is shown. Mean+/- stdev; * p<0.05. macroscopic images at the time of harvest are also shown. (**C-E**) Analysis of metabolic gene expression from a mouse single cell RNA-seq (scRNA-seq) dataset (*22*) represented as entire cell populations and comparing primary

pancreatic cancer (PDAC) and liver metastases (liver met) arising in the KPC model (C); UMAP plot comparing metabolic gene expression in single cells from primary PDAC, lung metastases (lung met), and liver metastases (liver met) in the KPC model (D); and the UMAP plot of metabolic gene expression analysis in D with each clonal populations represented; these clones are arbitrarily labeled as clones 1-6 and are do not represent clone numbers in the original publication (E). (**F**) Cross correlation of bulk metabolic gene expression profiles involving 3,240 genes from 620 samples with expression obtained from either hepatocellular carcinoma (HCC) TCGA, PDAC (Panc-seq), or PDAC TCGA data (top). Ranked metastatic samples with high degree of hepatocyte contamination as assessed by higher gene expression of hepatocyte markers and lower gene expression of ductal markers is shown on the bottom with corresponding correlation to normal liver.

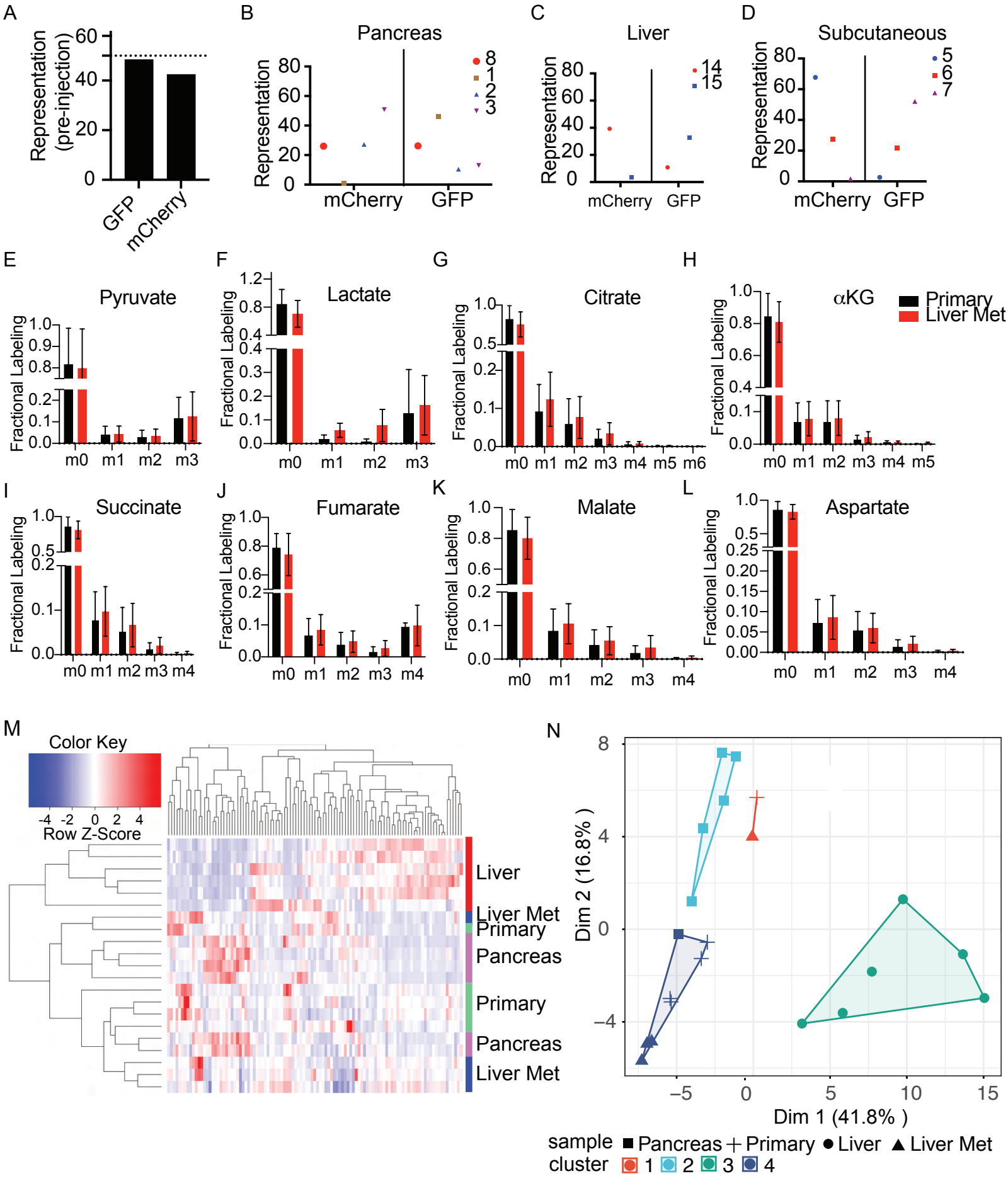

Figure 2

A

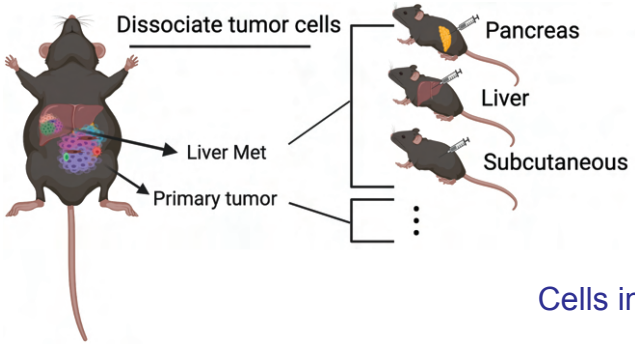

B

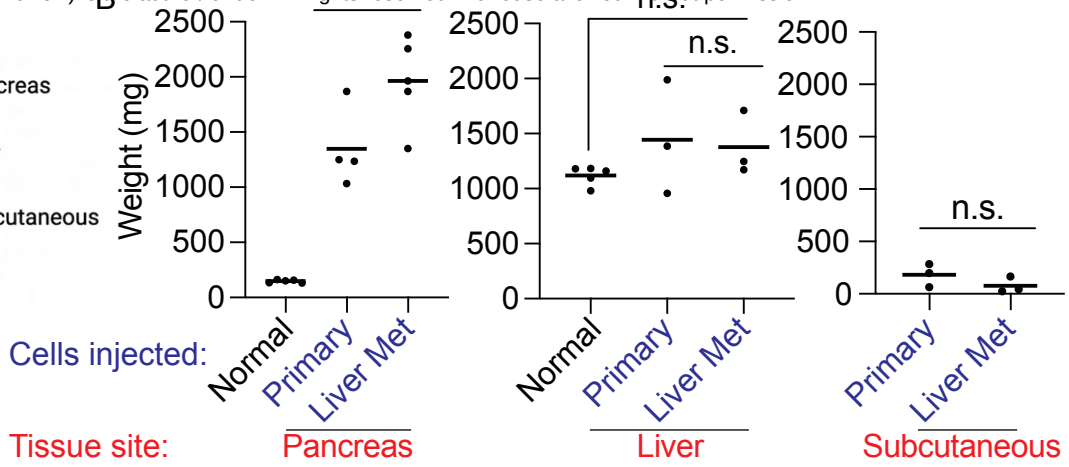

C

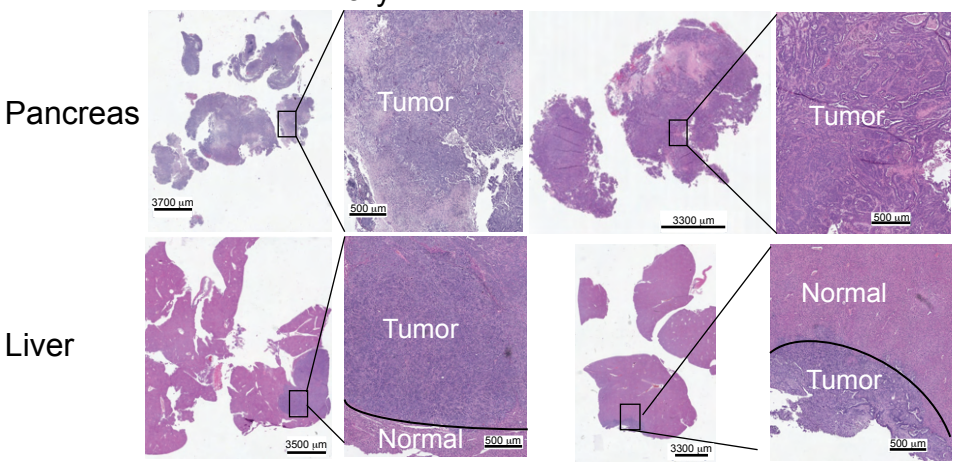

D

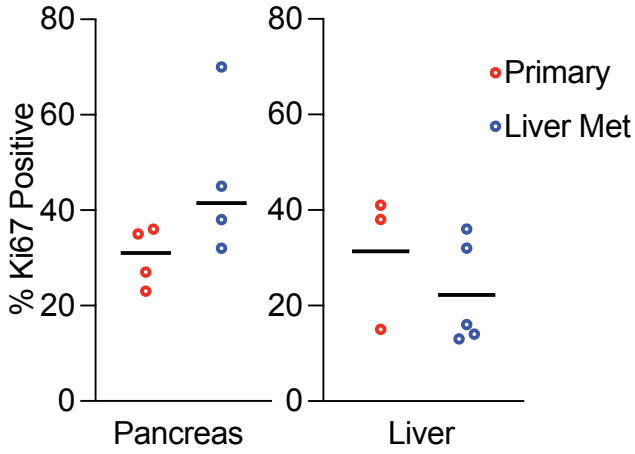

E

Pancreas

	Incidence P	Incidence M	Avg. Survival-days P	Avg. Survival-days M
10,000	3 (3)	3 (3)	36	38
1,000	3 (3)	3 (3)	49	46
100	5 (6)	4 (6)	68	94
10	0 (3)	0 (3)	-	-

F

Liver

	Incidence P	Incidence M	Avg. Survival-days P	Avg. Survival-days M
10,000	3 (3)	4 (4)	36	50
1,000	3 (3)	2 (5)	60	58
100	0 (3)	0 (3)	-	-

G

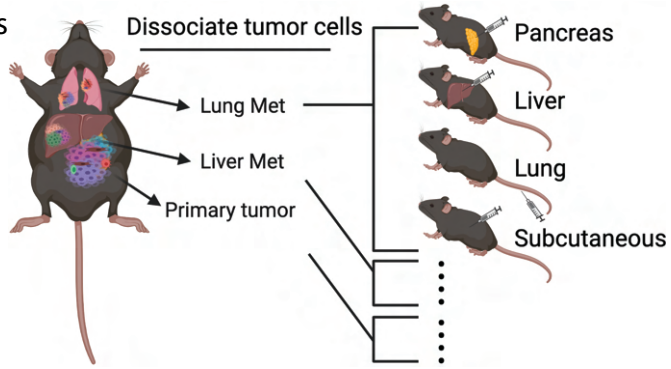

H

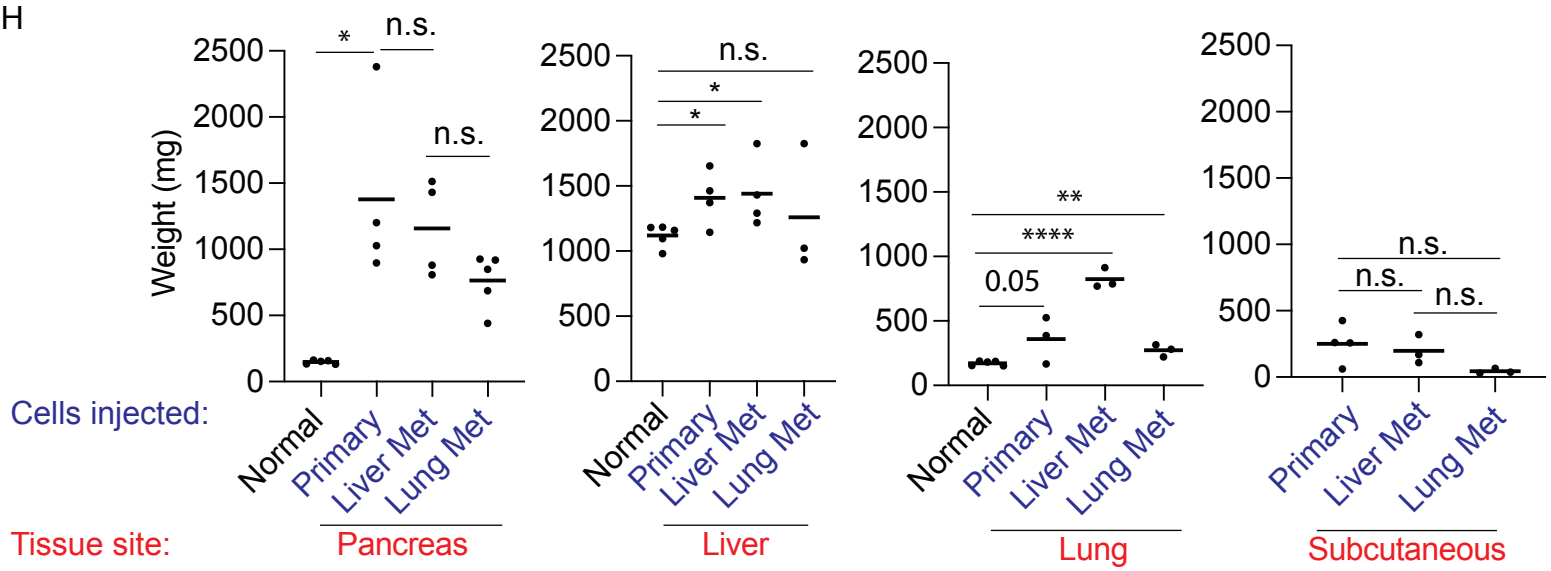

Figure 3

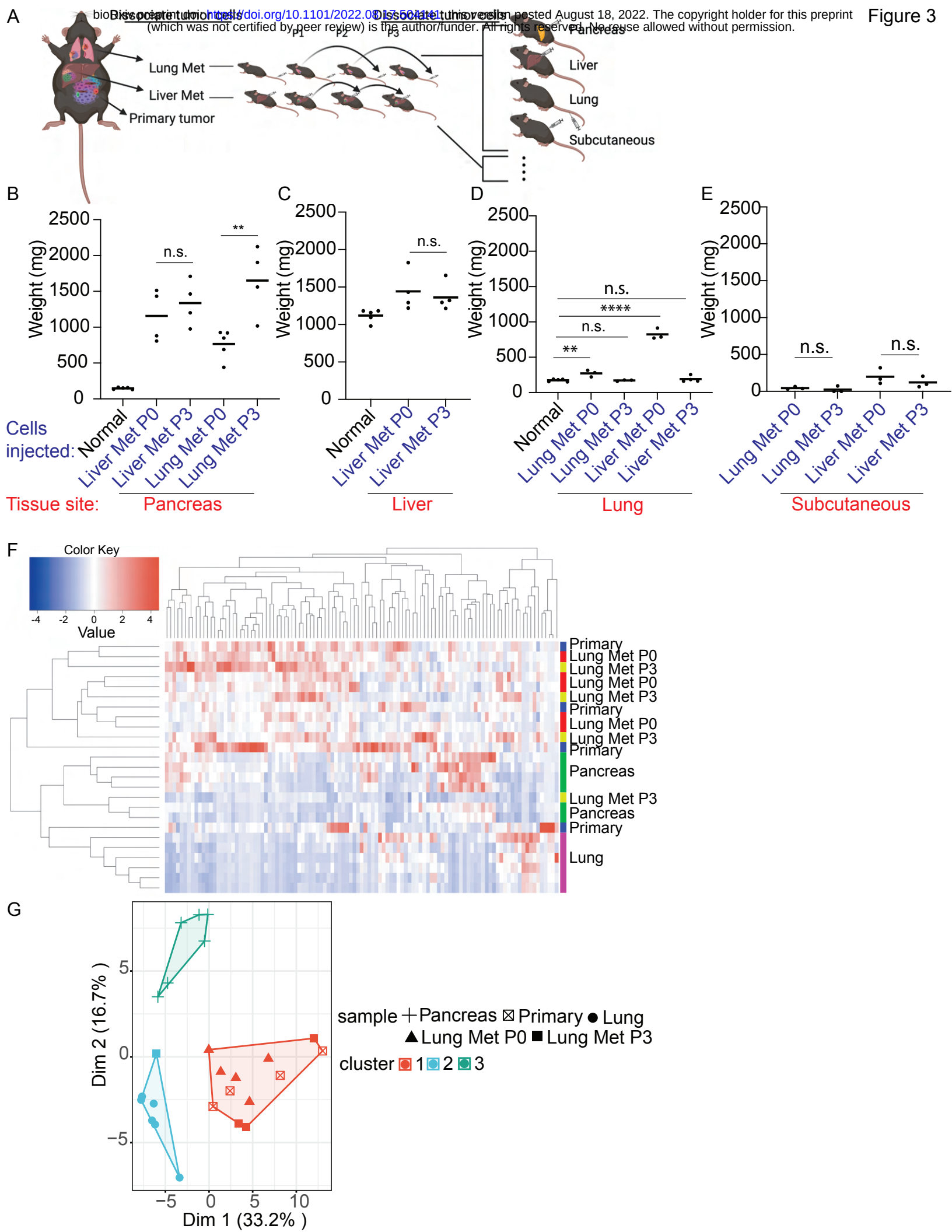

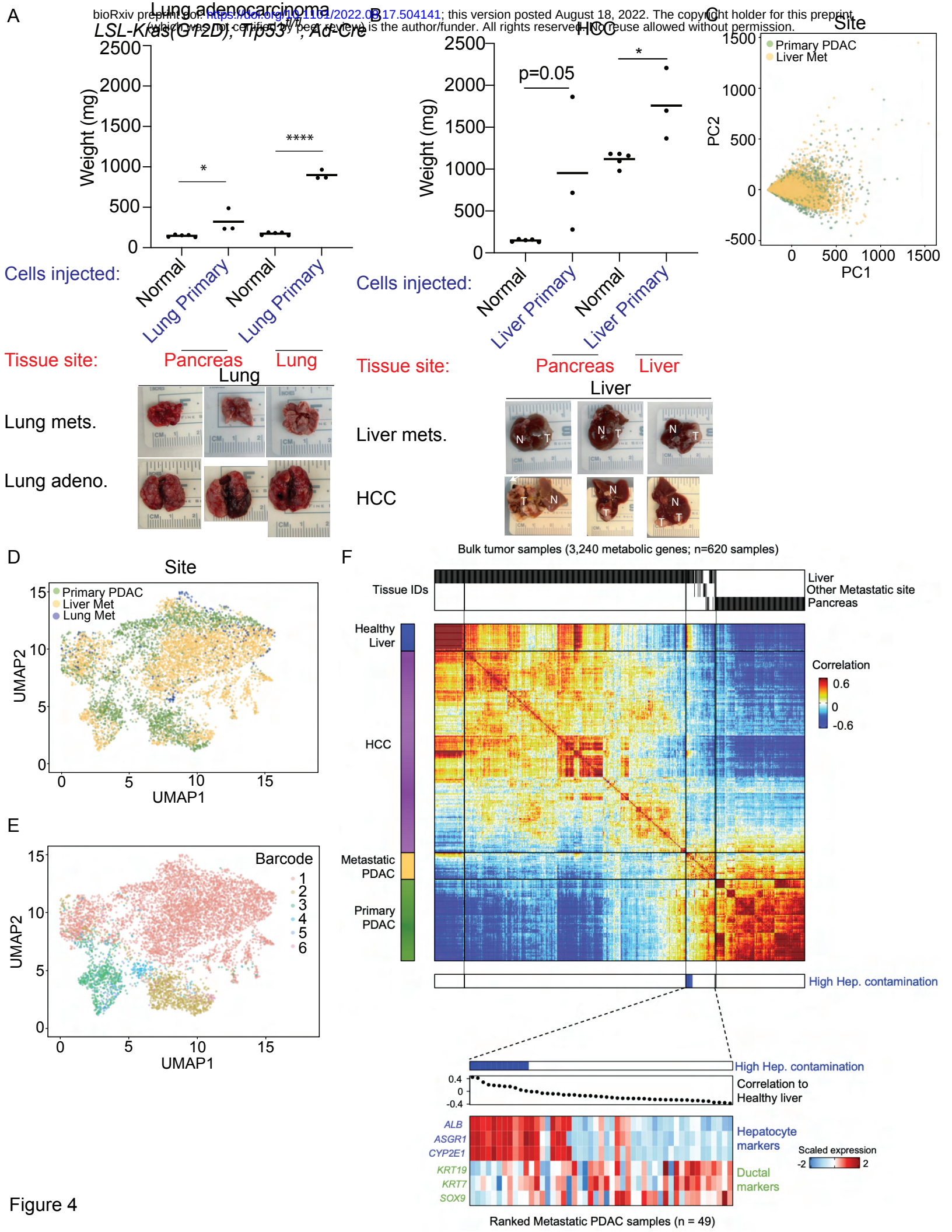

Figure 4